

Development and Preliminary Validation of an Efficient Alkali Metal Heat Pipe Analysis Model for Long Time Transient Simulations*

Chuntao Tang,¹ Kang Chen,^{1,†} Kaiyuan Zhu,² Guojun Hu,^{2,‡} Qichang Chen,¹ Chang Zhang,¹ Jinkun Zhao,¹ and Botong Dong¹

¹Shanghai Nuclear Engineering Research & Design Institute CO., LTD.

²School of Nuclear Science and Technology, University of Science and Technology of China, Hefei Anhui, China

Heat pipe cooled reactors are ideal for space power, military, and marine energy applications. A key aspect in the safety analysis of the heat pipe cooled reactor is the efficient modeling of heat pipes and their coupling with the solid reactor core. When a heat pipe begins in a cold state, the working substance within the vapor core transitions through several stages, moving from rarefied vapor flow to continuous vapor flow. This progression complicates the analysis of transient heat pipe behaviors. This work aims to develop a core analysis model for the heat pipe cooled reactor based on the coupling of ANSYS/Fluent and a newly developed transient heat pipe analysis code HePIRE-HA. A compressible two-equation model for the heat pipe vapor core is developed and solved alongside the heat pipe wall and wick through a fully-implicit solution scheme. A comprehensive interface tracking scheme has been developed to effectively manage the transition from a rarefied vapor state to a continuous vapor state. This transition scheme is demonstrated to work reasonably well and shows great efficiency. The coupling of ANSYS/Fluent and HePIRE-HA is achieved through the User Defined Function (UDF) capability of ANSYS/Fluent. A series of verification and validation studies is conducted to assess the performance and capabilities of the newly developed model. The results highlight that the new coupling model effectively predicts the transient response of the reactor core, making it a trustworthy tool for designing and ensuring the safety of the heat pipe cooled reactor.

Keywords: Heat Pipe; Micro Reactor; RETA; ANSYS.

I. INTRODUCTION

A heat pipe reactor, classified as a solid-state reactor, does not utilize a primary coolant loop to facilitate the transfer of heat from the core. Instead, it uses heat pipes to passively transfer heat from the core. This design confers numerous advantages for heat pipe cooled reactors, including ease of operation, miniaturization, and reliability[1]. Heat pipe reactors offer reliable nuclear energy for deep space exploration, remote areas, marine power, and floating platforms[2, 3].

A heat pipe is composed of the wall, working substance, and wick. It has very high thermal conductivity, allowing it to maintain an almost uniform temperature along its heated and cooled sections[4]. In practical applications, the frozen startup processes of a heat pipe involve intricate physical phenomena, including two-phase flow, phase change, and porous media flow[5]. These factors pose challenges for analyzing heat pipe reactors. Calculating and analyzing heat pipes are essential for the thermal design and safety evaluation of heat pipe reactors.

The heat pipe model can be divided into three types based on the modeling method of vapor flow in the vapor core: thermal resistance method[6], single-phase flow method[7], and two-phase flow method[8]. Among them, the thermal resistance method[6] considers heat pipes as a heat resistance network. This method has poor accuracy, and it is difficult to simulate the vapor flow state in heat pipes. The two-phase

flow method[8] is immature; the convergency issue makes it difficult to simulate the frozen startup processes of heat pipes. The single-phase flow model captures vapor flow characteristics effectively and converges better than the two-phase flow model. At present, the single-phase flow model[7] typically simulates the frozen startup of the heat pipe by determining the transition temperature of the continuum flow state; the rarefied vapor flow is typically ignored during the initial startup of the heat pipe.

This work will propose a new vapor flow model. In this new model, during the heat pipe's frozen startup, the vapor density in the core increases until reaching a steady state, undergoing three stages: vacuum, transition vapor flow, and continuum flow. The cylindrical heat pipe's angular symmetry allows for a two-dimensional modeling approach[9]. In this way, we can accurately and quickly simulate the frozen startup of a heat pipe. This new model and the heat pipe analysis code HePIRE-HA are developed on top of the generic code framework RETA[10].

The modeling of solid-state reactor cores can be divided into three types[11]: multi-channel one-dimensional models[12, 13], multi-channel two-dimensional models[14], and three-dimensional models[15]. The multi-channel and one-dimensional models are well suited for system-level safety analysis but compromise for computational accuracy [16–18]. In the contrast, the three-dimensional reactor core model is the most accurate but asks for the most computational resources. The primary objective of these work is the multi-physics simulations of the heat pipe reactors, and much progress has been made [19–24]. For example, Guo et al.[25] applied the lumped parameter method for modeling heat pipes in their heat pipe reactor simulations and utilized OpenFOAM to simulate the three-dimensional core. Lee et al.[26] utilized ANSYS to create a three-dimensional model of heat pipes and

* Supported by the National Natural Science Foundation of China (No. U20B2012) and the Nuclear Technology Research and Development Project (No. HNKF202303(42)).

† Corresponding author, chenkang1@snerdi.com.cn.

‡ Corresponding author, huguojun@ustc.edu.cn.

61 cores, allowing for a monolithic solution for the heat pipe re-
 62 actor. As heat pipes are modeled in two dimensions, the vapor
 63 flow control equation differs from the heat conduction con-
 64 trol equation for the core. Generally, the core section takes
 65 longer to resolve than the heat pipe section. The heat conduc-
 66 tion equation is simpler to solve than the vapor flow equation.
 67 Consequently, this paper employs the iterative method to an-
 68 alyze the coupling between the core and heat pipes.

69 This article is organized as follows: Section II introduces
 70 physics models and numerical solution framework of the heat
 71 pipe code HePIRE-HA; Section III presents the verification
 72 and validation of the heat pipe and coupling models; Section
 73 IV uses the developed heat pipe reactor thermal analysis pro-
 74 gram to conduct steady-state and transient thermal analysis
 75 of the KRUSTY reactor[27]; Section V discusses conclusions
 76 and future prospects.

77 II. MODEL DESCRIPTION

78 A. Heat pipe model

79 The study considers the conventional cylindrical heat
 80 pipes, which are composed of the heat pipe wall, wick, and
 81 vapor core regions. This work considers the compressible
 82 one-dimensional flow model for the vapor core. The one-
 83 dimensional vapor flow model will be coupled with a cylin-
 84 drical two-dimensional heat conduction model for the heat
 85 pipe wall and wick. The explicit coupling between the wick
 86 and vapor core is avoided by coupling them internally in this
 87 newly developed model.

88 As shown in Fig. 1, the startup process of a heat pipe[28]
 89 from a cold state can be divided into the following five stages:

- 90 1. When the heat pipe starts, the working substance in the
 91 wick is solid. The vapor core can be considered a vac-
 92 uum.
- 93 2. As heat continuously flows into the evaporator section
 94 of the heat pipe, the working substance in the wick be-
 95 gins to melt. Since the solid-liquid interface has not
 96 yet reached the interface between the wick and the vac-
 97 uum, there is no evaporation, and the vapor core
 98 remains in a vacuum state.
- 99 3. In the evaporator section, the working substance in the
 100 wick completely melts, and the fluid evaporates at the
 101 gas-liquid interface. At this time, the vapor pressure is
 102 very low, and the vapor core is in a state of rarefied vac-
 103 uum or transition vapor flow. In the adiabatic section and
 104 the condenser section, part of the working substance in
 105 the wick is still in a solid state.
- 106 4. As the evaporation process continues, the vapor accu-
 107 mulated in the vapor core becomes sufficient, and con-
 108 tinuum vapor flow begins from the evaporator section.
 109 Near the end of the condenser section, the vapor flow is
 110 still in a state of rarefied vapor or transition vapor flow,
 111 and the vapor core as a whole is in a transitional state.

5. The working substance in the wick completely melts,
 and the vapor core is entirely in a state of continuum
 vapor flow until it reaches a steady state.

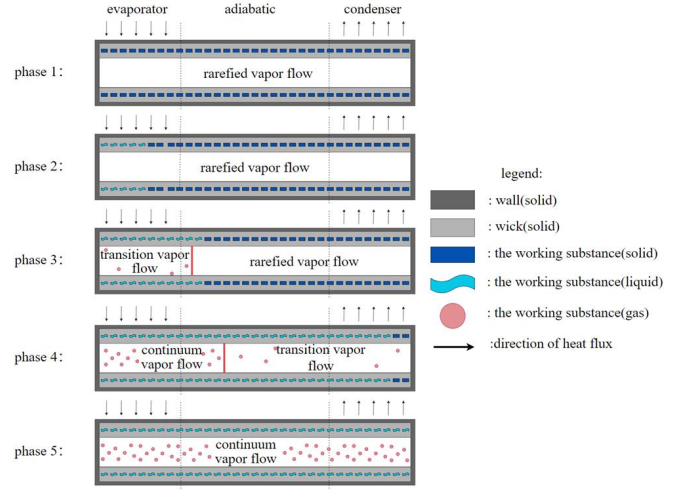


Fig. 1. Illustration of the startup process of a heat pipe from a frozen state.

115 The state of the working substance in the core region de-
 116 pends mainly on the density (and thus the temperature) of the
 117 vapor during the startup process. The dimensionless Knud-
 118 sen number (Kn), defined as the ratio of the molecular mean
 119 free path length to the vapor core diameter, is commonly used
 120 to determine the different phases of the vapor core. In this
 121 work, the vapor flow is identified as rarefied vapor flow when
 122 Kn is larger than 10 and as continuum vapor flow when Kn
 123 is smaller than 0.01. For the case $0.01 \leq Kn \leq 10$, the vac-
 124 uum flow could be a mixture of rarefied vapor flow, transition
 125 vapor flow, and continuum vapor flow. In the practical imple-
 126 mentation, the transition Knudsen number is converted to a
 127 transition temperature T^* using the kinetic theory of gases as
 128 follows:

$$\rho(T^*) = \frac{1.051\kappa}{\sqrt{2}\pi\sigma^2 R D \cdot Kn} \quad (1)$$

130 In which, ρ is the density of vapor, κ is the Boltzmann
 131 constant in the unit of J/K, σ is the Stefan-Boltzmann constant
 132 in the unit of W/(m² K⁴), R is the gas constant in the unit of
 133 J/(kg K), and D is the diameter of vapor core in the unit of
 134 m. Note that the transition temperature T^* may need to be
 135 solved iteratively using Equation (1) when the vapor Equation
 136 of State (EOS) is complex.

137 1. Heat pipe wall and wick model

138 The heat pipe wall and wick regions are modeled as a two-
 139 dimensional axisymmetric solid heat structure. The govern-
 140 ing equation for solid temperature is

$$\rho_s c_{p,s} \frac{\partial T_s}{\partial t} - \frac{1}{r} \frac{\partial}{\partial r} \left(r k_s \frac{\partial T_s}{\partial r} \right) - \frac{\partial}{\partial z} \left(k_s \frac{\partial T_s}{\partial z} \right) - q_s''' = 0 \quad (2)$$

In which subscript s represents solid. Note that solid density ρ_s , specific heat capacity $c_{p,s}$, and thermal conductivity k_s are all temperature-dependent. The nonlinearity due to this dependency is resolved by the fully-implicit solution scheme.

Given the high thermal conductivity of the liquid metal working substance and the thin wick thickness, the influence of liquid flow in the wick can be disregarded without introducing notable errors in the macroscopic average temperature of the wick structure[13]. We will disregard the liquid flow in

the wick structure and treat it as a solid region for heat conduction. The effective thermal conductivity will be assessed considering the wick structure's porosity, the thermal conductivity of the fluid, and the conductivity of the wick material. During the cold startup of the heat pipe, the effective properties of the wick structure are largely influenced by the wick's temperature, as this affects the melting of the working materials. In this work, the effective properties of wick structure are formulated as:

$$k_{s, \text{wick}}(T) = \begin{cases} k_{se} & T < T_m - \delta T \\ k_{se} + (k_{le} - k_{se}) \frac{T - T_m + \delta T}{2\delta T} & T_m - \delta T \leq T \leq \delta T + T_m \\ k_{le} & T > T_m + \delta T \end{cases} \quad (3)$$

In which T_m is the melting temperature of the working substance and δT is a controllable temperature interval. The effective thermal conductivity of the wick structure is transitioned from k_{se} to k_{le} when the wick temperature increases across the melting temperature. k_{se} and k_{le} is the effective thermal conductivity of the wick when the working substance is in the solid state and liquid state, respectively. This work focuses on the wrapped screen wick design where the effective thermal conductivity is affected by the porosity (φ):

$$k_{se} = \frac{k_1 [(k_1 + k_{SW}) - (1 - \varphi)(k_1 - k_{SW})]}{[(k_1 + k_{SW}) + (1 - \varphi)(k_1 - k_{SW})]} \quad (4)$$

$$k_{le} = \frac{k_2 [(k_2 + k_{SW}) - (1 - \varphi)(k_2 - k_{SW})]}{[(k_2 + k_{SW}) + (1 - \varphi)(k_2 - k_{SW})]} \quad (5)$$

In which k_1 and k_2 are the thermal conductivity of working substance in pure solid and liquid state, and k_{sw} is the thermal conductivity of screen material. Similarly, the effective heat capacity of the wick structure is

$$(\rho c_p)_{s, \text{wick}} = \varphi (\rho c_p)_2 + (1 - \varphi) (\rho c_p)_{ws} \quad (6)$$

In which $(\rho c_p)_2$ is the heat capacity of the working substance in a liquid state.

2. Continuum vapor flow model

A two-equation vapor flow model is employed when the vapor exists in a continuum state. Assuming the vapor flow is in saturation condition, the conservation equations for the vapor flow are formulated using the mass and momentum equation as,

$$\frac{\partial \rho}{\partial t} + \frac{\partial \rho u}{\partial z} - \Gamma = 0 \quad (7)$$

$$\frac{\partial \rho u}{\partial t} + \frac{\partial \rho u^2}{\partial z} + \frac{\partial p}{\partial z} + \frac{\lambda}{2D_h} \rho u |u| = 0 \quad (8)$$

In which Γ is the mass generation rate per unit volume, D_h is the hydraulic diameter of the vapor core region, and λ is the dimensionless friction coefficient.

The heat pipe vapor core is coupled with the wick's inner surface through a convection-like formula. A user-specified effective heat transfer coefficient h_v is used to couple the vapor core temperature T and solid temperature T_s by

$$q_s'' = -k_s \frac{\partial T_s}{\partial r} = h_v (T_s - T) \quad (9)$$

In which q_s'' is the heat flux at the wick-core interface. For the heat pipe, the heat transfer at the wick-core interface is, in fact, through the evaporation/condensation of the working substance. The mass generation rate Γ is computed from the heat flux by

$$\Gamma = \frac{a_w q_s''}{h_{fg}} \quad (10)$$

In which a_w is the heat transfer surface area density per unit volume and h_{fg} is the latent heat of evaporation/condensation.

This work considers mainly high-temperature alkali metal heat pipes with Sodium or Potassium as the working substance. Let T and p be the vapor temperature and pressure. The EOS of the vapor core material is modeled by a group of 5th-order polynomials, where the thermodynamic and mechanical properties of vapor are formulated as functions of the saturation temperature by

$$\begin{cases} \text{for density: } \ln(\phi) = \sum_{m=0}^5 A_m T_v^m \\ \text{for other properties: } \phi = \sum_{m=0}^5 A_m T_v^m \end{cases} \quad (11)$$

In which ϕ represents a thermodynamic or mechanical property of the vapor. The coefficients A_m for the Sodium [30] and Potassium [31] are listed in Table 1 for reference.

In the current formulation, the vapor is assumed to be in the saturated condition, and the Clausius-Clapeyron equation is used to determine the vapor saturation temperature from the vapor pressure,

Table 1. Coefficients of fitting polynomials for Sodium and Potassium.

	Properties	A ₀	A ₁	A ₂	A ₃	A ₄	A ₅
Sodium:371K-1800K	Pressure	-5.73e+03	1.81e+01	-2.25e-02	1.52e-05	-5.30e-09	7.50e-13
	Density	-5.76e-02	1.82e-04	-2.29e-07	1.56e-10	-5.51e-14	7.86e-18
	Heat capacity	-9.50e+03	3.49e+01	-3.25e-02	8.57e-06	2.28e-09	-1.03e-12
	Heat conductivity	8.88e-02	-4.50e-04	1.12e-06	-1.04e-09	4.41e-13	-7.12e-17
	Viscosity	6.54e-06	1.27e-08	-3.93e-12	1.52e-14	-1.08e-17	2.36e-21
Potassium:600K-1500K	Pressure	-6.08e+06	2.01e+04	-2.96e+01	-2.39e-02	-1.00e-5	1.71e-9
	Density	-4.39e-02	1.51e-04	-1.99e-07	1.45e-10	-5.60e-14	8.86e-18
	Heat capacity	1.11e+02	-8.17e-01	2.65e-03	-3.15e-06	1.63e-09	-3.15e-13
	Heat conductivity	6.09e-02	-3.49e-04	8.01e-07	-7.97e-10	3.77e-13	-6.92e-17
	Viscosity	-8.41e-06	6.35e-08	-8.34e-11	5.98e-14	-1.52e-17	1.28e-32

$$\frac{dp}{p} = \frac{h_{fg}}{R} \frac{dT}{T^2} \quad (12)$$

With vapor temperature as the dependent variable, the vapor density is formulated as

In which h_{fg} is the specific enthalpy of vaporization. In practice, given the reference temperature T_c and reference pressure p_c , the saturation temperature is derived as

$$\rho = \frac{p_c}{RT} \exp \left[\frac{h_{fg}}{R} \left(\frac{1}{T_c} - \frac{1}{T} \right) \right] \quad (15)$$

$$\frac{1}{T} = \frac{1}{T_c} - \frac{R}{h_{fg}} \ln \frac{p}{p_c} \quad (13)$$

Using the Clausius-Clapeyron equation, the pressure gradient term in Equation (8) is transformed into

A closed-form friction coefficient correlation is required to correctly predict the flow field in the vapor core region. The friction coefficient λ in Equation (8) depends on the Reynolds number. In this study, the friction coefficient is modeled as

$$\frac{\partial p}{\partial z} = \frac{dp}{dT} \frac{\partial T}{\partial z} = \frac{\rho h_{fg}}{T} \frac{\partial T}{\partial z} \quad (14)$$

$$\lambda = \begin{cases} \frac{64}{Re} & Re \leq 2200 \\ 0.0291 + 1.7 \times 10^{-5}(Re - 2200) & 2200 < Re < 3000 \\ \frac{0.316}{Re^{0.25}} & Re > 3000 \end{cases} \quad (16)$$

B. Rarefied vapor flow model

The density of vapor in the Rarefied state is quite small, and heat transfer through Rarefied vapor flow is negligible. In this work, the Rarefied vapor flow region is treated as a vacuum region. In the practical implementation, the vapor velocity at the Rarefied transition boundary is set to zero. When the heat pipe temperature rises, the Rarefied transition boundary moves smoothly along the heat flow direction until it reaches the condenser end.

In which Γ is the mass generation rate per unit volume. In which D_K is the diffusion coefficient[29] of the vapor calculated by

$$D_K = \frac{2R_v}{3} \bar{v} = \frac{2R_v}{3} \sqrt{\frac{8\kappa T}{\pi m_g}} \quad (18)$$

In which R_v is the radius of the vapor core, \bar{v} is the average molecular speed, and m_g is the molecular mass of the vapor.

1. Transition vapor flow model

When the flow in the vapor core is in the Transition vapor state, the vapor density and mass flux are not negligible. The heat flux brought by the Transition vapor flow helps heat up the remaining cold region. For simplicity, a diffusion model is used in this work to model the Transition vapor flow, i.e.

$$\frac{\partial \rho}{\partial t} - \frac{\partial}{\partial z} \left(D_K \frac{\partial \rho}{\partial z} \right) - \Gamma = 0 \quad (17)$$

2. Heat pipe boundary conditions

Flexible boundary conditions are available for the heat pipe evaporator and condenser outer wall, including temperature, heat flux, convection, and radiation boundary conditions. At both ends of the heat pipe, the velocity and temperature gradient of vapor flow are set to zero. During the startup stage, the mass flux at the boundary of different vapor flow regions is set according to the flow conditions. At the Rarefied-Transition boundary, the mass flux is set to zero; at the Transition-Continuum boundary, the mass flux is set to the diffusive

269 $\text{flux}(\rho u)$.

270 C. Heat pipe solution method

271 The heat pipe model has been integrated into the
272 RETA system thermal-hydraulics code framework[10], which
273 provides fundamental capabilities like nonlinear equation
274 solvers, component design, physical module design, and IOs.
275 A HeatPipe component and the associated discretization ob-
276 jects are added to achieve the previously described heat pipe
277 models, as shown in Fig. 2.

278 The governing equations for heat pipes are discretized us-
279 ing the Finite Volume Method (FVM) on structured, orthogo-
280 nal grids. The Backward Discretization Formula is employed
281 for the transient terms. Following the temporal and spatial
282 discretization, a set of coupled Nonlinear Algebraic Equa-
283 tions (NAEs) is generated. Nonlinearity is unavoidable and
284 will be resolved iteratively using a Newton-type nonlinear
285 equation solver.

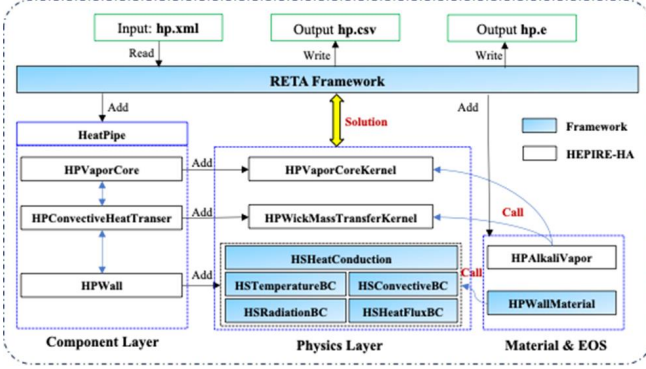


Fig. 2. The structure of the heat pipe analysis code HePIRE-HA.

287 Let \mathbf{x} be the unknown solution and \mathbf{R} be the residual vector
288 of the system of NAEs:

$$290 \quad \mathbf{R}(\mathbf{x}) = \mathbf{0} \quad (19)$$

291 The Newton's method (with a line search algorithm) solves
292 the system of NAEs iteratively by:

$$293 \quad \mathbb{J}(\mathbf{x}_k) \cdot \delta \mathbf{x} = -\mathbf{R}(\mathbf{x}_k) \quad (20)$$

$$294 \quad \mathbf{x}_{k+1} = \mathbf{x}_k + \alpha \cdot \delta \mathbf{x} \quad (21)$$

296 in which k is the nonlinear iteration index, \mathbb{J} is the system
297 Jacobian matrix, and α is the line search relaxation factor.
298 Equation (20) can be solved with either a direct or an it-
299 erative linear equation solver. A Preconditioned Jacobian-
300 Free Newton-Krylov (PJFNK) solver is developed to reduce
301 the burden of calculating the exact Jacobian matrix. In the
302 PJFNK method, Equation (20) is replaced by

$$303 \quad \mathbb{A} \cdot \mathbf{y} = -\mathbf{R}(\mathbf{x}_k) \quad (22)$$

$$305 \quad \mathbb{A} \equiv \mathbb{D}(\mathbf{x}_k) \cdot \mathbb{P}^{-1}, \mathbf{y} \equiv \mathbb{P} \cdot \delta \mathbf{x} \quad (23)$$

306 in which \mathbb{A} is the right-preconditioned Jacobian matrix and \mathbb{P}
307 is the preconditioning matrix. In the PJFNK method, Equa-
308 tion (22) is solved with a Krylov subspace solver. To address
309 convergence issues, an automatic time step size adjustment
310 algorithm is included in the solver. If the nonlinear solver
311 fails to converge, the time step size is reduced by half. This
312 approach is vital to enhance the solver's robustness during
313 long-term simulations.

314 D. Coupling interface

315 This work considers modeling the reactor core with the
316 ANSYS/Fluent software[32]. A coupling interface is created
317 with the UDF module from ANSYS. The reactor core and
318 heat pipes are coupled at the outer surface of the heat pipe
319 evaporator via convective heat transfer. As described in the
320 previous section, the heat pipe is modeled with an axisym-
321 metric 2D model. The dimension mismatch at the coupling
322 boundaries, i.e., 2D and 1D in the reactor core and heat pipe,
323 is the main difficulty in designing the coupling interface. As
324 shown in Fig. 3, a pseudo fluid with no heat capacity is added
325 to facilitate the coupling and data exchange between the re-
326 actor core and heat pipes. The boundary involves the exchange
327 of heat flux and the wall surface temperature of the heat pipe
328 evaporator. Users can specify an equivalent heat transfer co-
329 efficient to indicate the thermal resistance between the reactor
330 core and the heat pipe wall.

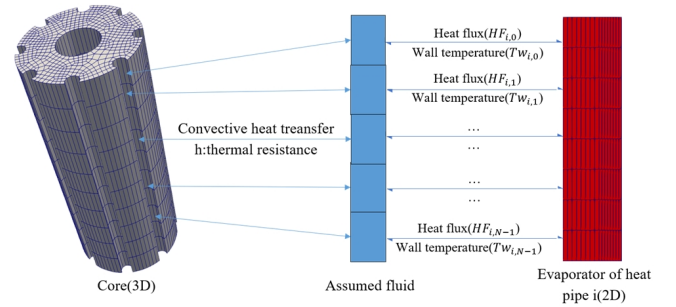


Fig. 3. Schematic of the coupling interface between ANSYS/Fluent and HePIRE-HA.

332 In the ANSYS reactor core model, a convective bound-
333 ary condition is set at the coupling boundary by utilizing
334 the temperature of the heat pipe wall surface. The heat flux
335 at this boundary is calculated and then relayed to the heat
336 pipe model. In the HePIRE-HA heat pipe model, a heat flux
337 boundary condition is applied at the coupling boundary, and
338 the heat pipe surface temperature is computed and transferred
339 to the reactor core model. The operator splitting technique
340 facilitates iterations between the core model and the heat pipe
341 model.
342

III. MODEL VERIFICATION AND VALIDATION

Table 2. Physical and boundary conditions for the heat pipe steady-state validation test cases.

Parameters	Case 1	Case 2
Fluid	Sodium	Sodium
P_c : Pa	1300	2476
T_c : K	818	856
$k_{s,wall}$: W/m · K	19.0	19.0
$k_{s,wic}$: W/m · K	66.2	66.2
R_v : m	0.007	0.007
δ_{wick} : m	0.001	0.001
δ_{wall} : m	0.005	0.005
h_v : W/m ² · K	1.0E+6	1.0E+6
Q : W	560	1000
h_{sink} : W/m ² · K	59.6	62.6
T_{sink} : K	300	300
Number of axial elements	80	112

A. Heat pipe steady-state model validation

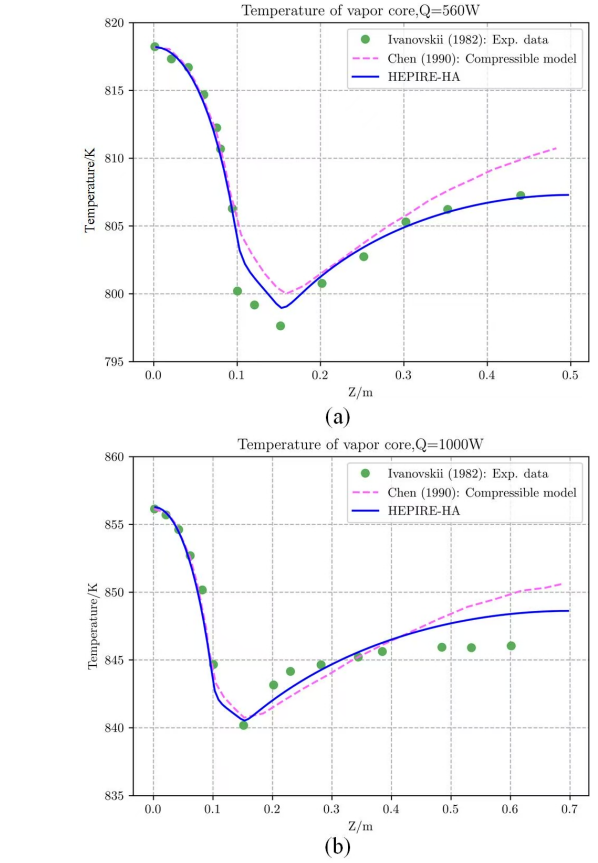


Fig. 4. The axial vapor temperature profile for the sodium heat pipe with $Q = 560$ W, (b)The axial vapor temperature profile for the sodium heat pipe with $Q = 1000$ W.

B. Heat pipe startup model validation

Following the steady-state operation validation study, a transient frozen startup validation study was conducted using the cylindrical sodium heat pipe experiments conducted by Faghri and co-authors[35]. Besides the experimental data, simulation results from Yoo[6] are also used as reference re-

sults for a code-to-code comparison. In Yoo's simulation model, a thermal resistance network was constructed based on the frozen startup model. The physical and boundary conditions for this test case are listed in Table 3.

In this experiment test, the heat pipe wall temperature at several axial spots was measured at different times. The heat pipe started with a cold temperature of 300 K and took heat from the resistance heaters. To account for the additional heat capacities of the resistance heaters and radiation shields, an estimated heat capacity of $3.75 \times 10^6 \text{ J} / (\text{m}^3 \cdot \text{K})$ is added to the heat pipe wall.

Table 3. Physical and boundary conditions for the heat pipe frozen startup test.

Parameters	value	Parameters	value
L_e : (mm)	93.0	Fluid	Sodium
L_a : (mm)	188.0	Wick material	SS304
L_c : (mm)	500.0	Wall material	SS304
R_v : mm	10.75	Porosity	0.7
δ_{wick} : mm	0.5	Emissivity	0.645
δ_{wall} : mm	1.0	Power: W	112

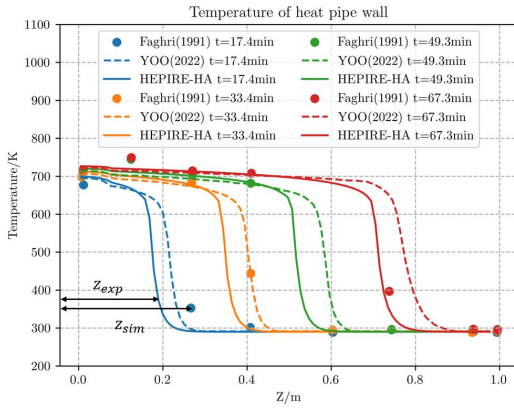


Fig. 5. Comparison of heat pipe wall temperature profile for the frozen startup test.

As shown in Fig. 5, from 17.4 minutes to 67.3 minutes, as heat flux was applied to the heat pipe evaporator wall, the thermal front gradually moved towards the condenser. The prediction of wall temperature during the transient by HePIRE-HA matches the experiment data reasonably well but shows a non-negligible discrepancy in capturing the frozen interface, which indicates that the current treatment of the vapor flow under different conditions may need further improvement. Note that the reference simulation results showed similar discrepancies in predicting the frozen interface. In the current model, the condition of vapor flow is determined by the transition temperatures, which are fixed values determined by the vapor core diameter and transition Kn number. The code determines the interface between different vapor states by the transition temperature and gives a sharp discontinuity across the interface. In reality, the frozen interface is much smoother along the axial direction. And the assumption that the heat flux is uniformly distributed in evaporator surface causes the

discrepancy between simulation result and experimental result. For this case, the average computation time per time step on an AMD R7 9800X CPU is about 3.3 ms per time step. And the time step is 0.5 s.

C. Coupling model verification

A made-up fuel cell consists of a cylindrical fuel region and a central heat pipe is used to verify the coupling model. The schematic of this fuel cell is shown in Fig. 6(a). The fuel region is a cylindrical shell with an inner and outer radius of 0.5 m and 1.0 m, respectively. The fuel inner surface is coupled to a cylindrical heat pipe evaporator surface; a fixed temperature (T_{out}) is applied at the fuel outer surface. A convective boundary condition is applied at the heat pipe condenser surface with a fixed ambient heat transfer coefficient (h_{amb}) and ambient temperature (T_{amb}). A constant thermal conductivity is used for the fuel region (k_{fuel}) and heat pipe wall (k_{HP}). Detailed physical and boundary conditions are listed in Table 4.

Table 4. Physical and boundary conditions for the fuel cell verification test.

Parameters	value	Parameters	value
L_e : mm	400.0	H : mm	400.0
L_a : mm	400.0	k_{HP} : W / ($\text{m}^2 \cdot \text{K}$)	30.0
L_c : mm	200.0	k_{fuel} : W / ($\text{m}^2 \cdot \text{K}$)	0.2
R_v : mm	10.0	T_{out} : K	1009.9
δ_{wick} : mm	0.5	h_{amb} : W / ($\text{m} \cdot \text{K}$)	20.0
δ_{wall} : mm	1.5	T_{amb} : K	650.0

For this test case, the temperature distribution in the fuel cell can be derived analytically by assuming that the temperature drop across the heat pipe vapor core is negligible, i.e. the total thermal resistance of the heat pipe is mainly determined by the thermal resistance of the heat pipe wall.

Though this is a very simple test condition, it is useful for verifying the coupling model. Fig. 6(b) shows the comparison of radial fuel temperature distribution from code prediction and the analytical result. The agreement is excellent with negligible discrepancy, the relative error between the analytical result and the simulated result is less than 0.1%.

Besides the simulation results, the convergence of the coupling model is another importance key factor to assess. In this test, the convergence history of the total heat flow and the heat pipe evaporator wall temperature is recorded and presented in Fig. 6(c) and Fig. 6(d). It is observed that the coupling model is convergent. In terms of the convergence rate, it takes about 50 iterations to reduce the relative error by 2 order of magnitude. This convergence rate is not excellent and this is an area for future improvement.

IV. DEMONSTRATION

A heat pipe cooled reactor unit is selected to demonstrate and assess the performance of the previously developed cou-

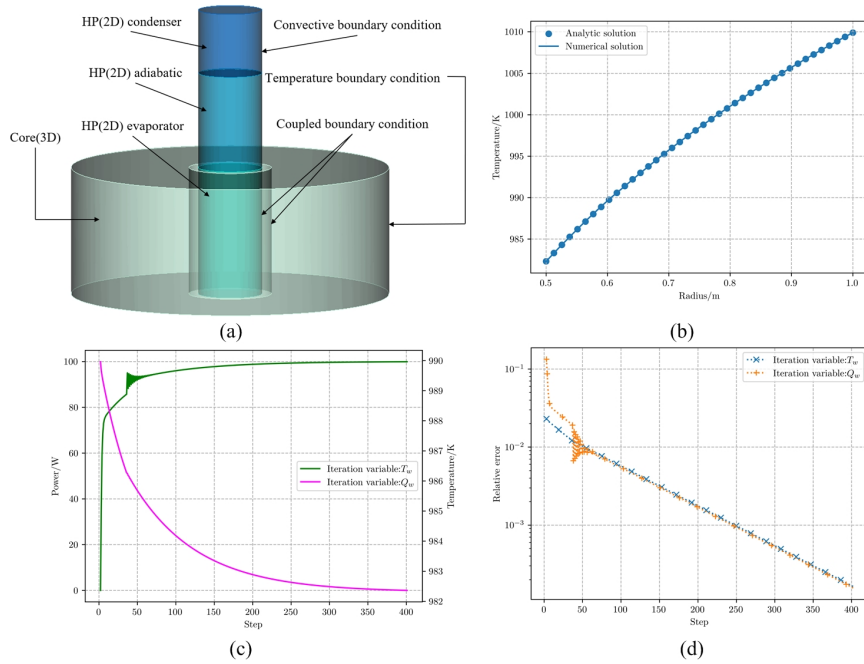


Fig. 6. (a) Schematic of the made-up fuel cell, (b) Radial temperature distribution in the fuel cell predicted by the coupling model, (c) Radial temperature distribution in the fuel cell predicted by the coupling model, (d) Convergence history of iteration variables.

plung model. The KRUSTY reactor[27] is a demonstration reactor for the design, development, and testing of kilowatt-level reactors. The KRUSTY reactor has a rated thermal power of 5 kW and generates 1 kW of electric power through a Stirling energy conversion device. The reactivity is controlled by a moving axial reflector and a central control rod. The schematic diagram of the reactor is shown in Fig. 7(a). The clamp provides clamping force to ensure close contact between the heat pipe and the fuel. The heat pipe wall material is Haynes 230 alloy. Up to now, several tests and experiments such as steady-state operation, load following, and startup have been conducted on the KRUSTY reactor. A load following test[36] of the KRUSTY reactor program is selected to demonstrate and validate the newly developed coupling model. This study is conducted in two steps.

In the first step, the steady-state operation of the reactor is simulated. The reactor core is modeled by ANSYS with the volumetric heating power density calculated by the OpenMC software[37]. For the steady-state operation, the total reactor power is 2678 W. The heat pipes are modeled by the HePIRE-HA code. The temperature at the heat pipe condenser outer wall surface is set at 1064 K, and it's the boundary condition of heat pipes. The following is a discussion of the computational results. The Temperature and Mach number of vapor flow for the heat pipe is shown in Fig. 7(c). The maximum of Mach number of vapor flow is 0.016, and the mean temperature of the heat pipe evaporator outer wall is 1066.9 K, meaning that there is a temperature rise of 2.9K from the heat pipe condenser outer wall to the evaporator outer wall. The fuel temperature distribution is the main quantity of interest and is shown in Fig. 7(b). The maximum fuel temperature is about 1082.5 K, meaning that there is a temperature drop of 17.5

K from the fuel center to the heat pipe condenser outer wall. This reflects the excellent heat transport capability of the heat pipes. However, since the thermal resistance between the fuel and heat pipe wall is not considered, the realistic temperature drop could be higher.

In the second step, a load following transient is simulated by restarting from the steady-state simulation. At the start of this transient process, it is assumed that the external load has dropped by 20%, meaning that the total heat removed by the heat pipes dropped suddenly from the steady-state 2678 W to 2117 W.

The reactivity feedback from fuel temperature change must be modeled to simulate accurately this load following transient. The point kinetics equation model from the RETA code is used to predict the transient reactor power. In this study, the reactivity feedback due to fuel temperature change and Sodium redistribution in the heat pipes are considered. In this study, the fuel temperature reactivity coefficient and reactor power reactivity coefficient are calculated by Postan[36], and the fuel temperature reactivity coefficient is -0.2825 cents/K. The Sodium redistribution is mainly affected by the input power in the evaporator of heat pipes; a reactor power reactivity coefficient of -0.0015 cents/W is used.

This transient simulation is performed using the coupling model, and the results are shown in Fig. 7(d). The reactor power, average fuel temperature, and total reactivity during the transient are presented. At time 0s, due to the sudden drop in external load, the total heat removed by heat pipes drops while the reactor power remains unaffected. This results in a short-term increase in fuel temperature. Then, the reactor power drops due to the negative fuel temperature reactivity feedback. After the reactor power drops to a certain

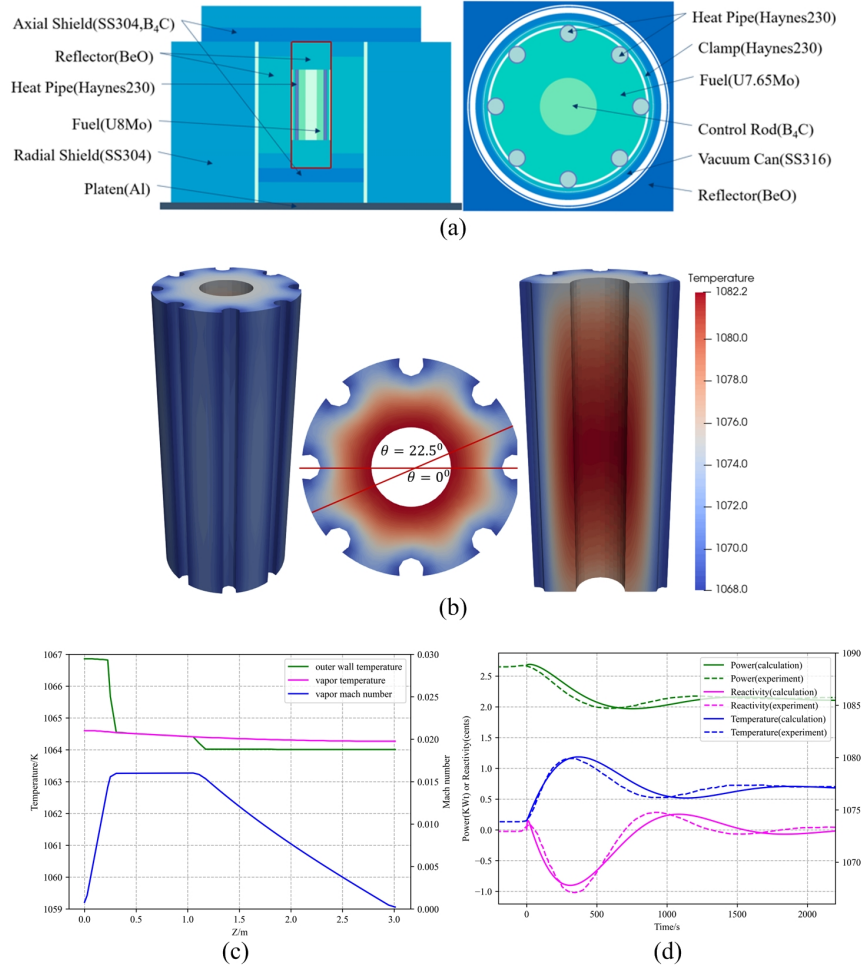


Fig. 7. (a) Schematic of the KRUSTY heat pipe reactor, (b) Steady-state fuel temperature distribution, (c) the axial temperature and Mach number for the sodium heat pipe, (d) Profile of reactor power, average fuel temperature, and total reactivity during the load following transient.

level, the reactor power starts to increase again due to the Sodium redistribution effect **i.e. reactor power reactivity feedback**. The combination of fuel temperature and Sodium redistribution reactive feedback causes oscillations in both the reactor power and the fuel temperature. After about 2000s following the start of this transient, the reactor power stabilized to a lower level consistent with the external load power 2.17kW, the average fuel increased about 3K. In this way, positive reactivity caused by fuel temperature increase is equal to negative reactivity caused by reactor power decrease. It is observed that the prediction by the coupling model matches the experimental data reasonably well. However, there is a visible discrepancy between the model prediction and experimental data. The uncertainty in the predictions could be large due to assumptions and simplifications made when developing this new model, e.g., Assumptions of the Point Reactor Kinetics Equations, simplification of the reactor core geometry, idealized boundary conditions at the heat pipe condenser surface, etc.

V. CONCLUSION AND FUTURE WORK

To conclude, this work develops an efficient high-temperature alkali metal heat pipe analysis code (HePIRE-HA). HePIRE-HA leverages the highly flexible code structure and highly efficient numerical solution schemes of the RETA advanced system analysis software. A compressible two-equation model for the heat pipe vapor core is developed, which is capable of simulating both steady-state operation and transient startup of the heat pipes. A validation study with both steady-state and frozen startup experiment data shows that the HePIRE-HA code is accurate and robust enough to handle the complex behaviors happening inside heat pipes. The computation efficiency of the HePIRE-HA code is excellent, making it quite suitable for long-time transient simulations as commonly required by reactor design and safety analysis studies.

In addition to the standalone heat pipe analysis software, a coupling interface is developed using the ANSYS UDF module to model and simulate the HP MicroRx reactor core. Using a pseudo fluid with zero heat capacity, the coupling inter-

face successfully resolves the issues caused by the mismatch in the dimensions at the coupling boundary. The coupling model is verified by studying a made-up fuel cell test case and validated by the KRUSTY load following test.

Results from the V&V and demonstration studies show that the heat pipe analysis model is reliable, robust, and efficient. However, results also show that the current heat pipe analysis model needs further improvement to capture more accurately the frozen startup boundary in the vapor core by using more accurate Rarefied vapor flow model. The convergence rate of the current coupling model could be significantly improved

to accelerate the computation of the reactor core analysis by using relaxed picard iteration.

ACKNOWLEDGEMENT

This work was supported by the National Natural Science Foundation of China (No. U20B2012) and the Nuclear Technology Research and Development Project (No. HNK202303(42))

- [1] H. Gu, Z. Shouzhi, Overview of space nuclear reactor power technology. *Journal of Deep Space Exploration* 4, 5 (2017). <https://doi.org/10.15982/j.issn.2095-7777.2017.05.004>.
- [2] Z. Anwen, L. Lei, M. Shijun, et al., An overview of the use and development of nuclear power system in deep space exploration. *Journal of Deep Space Exploration* 4, 5 (2017). <https://doi.org/10.15982/j.issn.2095-7777.2017.05.001>.
- [3] H. Yu, Z. Zhang, X. Chai, et al., Initiation and development of heat pipe cooled reactor. *Nuclear Power Engineering* 40, 4 (2019). <https://doi.org/10.13832/j.jnpe.2019.04.0001>.
- [4] A. Faghri, Review and advances in heat pipe science and technology. *J. Heat Transfer* 134, 12 (2012). <https://doi.org/10.1115/1.4007407>.
- [5] B. Zohuri, Heat pipe design and technology: Modern applications for practical thermal management. (Springer2016).
- [6] J. S. Yoo, M. Song, S. Qin, et al., A conduction-based heat pipe model for analyzing the entire process of liquid-metal heat pipe startup. Tech. rep., Idaho National Lab.(INL), Idaho Falls, ID (United States), (2022). <https://www.osti.gov/biblio/1856343>.
- [7] J. E. Hansel, C. d. S. B. Dutra, L. Charlot, et al., The liquid-conduction, vapor-flow heat pipe model in Sockeye. *Nucl. Eng. Des.* 426 (2024). <https://doi.org/10.1016/j.nucengdes.2024.113359>.
- [8] J. E. Hansel, R. A. Berry, D. Andrs, et al., Sockeye: A one-dimensional, two-phase, compressible flow heat pipe application. *Nucl. Technol.* 207, 7 (2021). <https://doi.org/10.1080/00295450.2020.1861879>.
- [9] G. Hu, Development of Heat Pipe Modeling Capabilities in a Fully-Implicit Solution Framework. International Conference Pacific Basin Nuclear Conference, (Springer, 2022). https://doi.org/10.1007/978-981-99-1023-6_72.
- [10] G. Hu, Development of a Fully-Implicit Second-Order system Thermal-Hydraulics analysis code for reactor modeling and simulations. *Nucl. Eng. Des.* 415 (2023). <https://doi.org/10.1016/j.nucengdes.2023.112715>.
- [11] C. Mueller, P. Tsvetkov, A review of heat-pipe modeling and simulation approaches in nuclear systems design and analysis. *Ann. Nucl. Energy* 160 (2021). <https://doi.org/10.1016/j.anucene.2021.108393>.
- [12] Y. Ma, J. Liu, H. Yu, et al., Coupled irradiation-thermal-mechanical analysis of the solid-state core in a heat pipe cooled reactor. *Nucl. Eng. Technol.* 54, 6 (2022). <https://doi.org/10.1016/j.net.2022.01.002>.
- [13] Z. Zhang, C. Wang, K. Guo, et al., HEART, a specific code for thermal-electrical analysis of heat pipe cooled nuclear reactor. *Int. J. Therm. Sci.* 179 (2022). <https://doi.org/10.1016/j.ijthermalsci.2022.107666>.
- [14] C. Wang, H. Sun, S. Tang, et al., Thermal-hydraulic analysis of a new conceptual heat pipe cooled small nuclear reactor system. *Nucl. Eng. Technol.* 52, 1 (2020). <https://doi.org/10.1016/j.net.2019.06.021>.
- [15] L. M. Alawneh, R. Vaghetto, Y. Hassan, et al., Conceptual design of a 3 MWth yttrium hydride moderated heat pipe cooled micro reactor. *Nucl. Eng. Des.* 397 (2022). <https://doi.org/10.1016/j.nucengdes.2022.111931>.
- [16] L. Ge, H. Li, X. Tian, et al., Improvement and validation of the system analysis model and code for heat-pipe-cooled microreactor. *Energies* 15, 7 (2022). <https://doi.org/10.3390/en15072586>.
- [17] C. Wang, H. Sun, S. Tang, et al., Thermal-hydraulic analysis of a new conceptual heat pipe cooled small nuclear reactor system. *Nucl. Eng. Technol.* 52, 1 (2020). <https://doi.org/10.1016/j.net.2019.06.021>.
- [18] Z. Zhang, C. Wang, K. Guo, et al., HEART, a specific code for thermal-electrical analysis of heat pipe cooled nuclear reactor. *Int. J. Therm. Sci.* 179 (2022). <https://doi.org/10.1016/j.ijthermalsci.2022.107666>.
- [19] Y. Ma, C. Tian, H. Yu, et al., Transient heat pipe failure accident analysis of a megawatt heat pipe cooled reactor. *Prog. Nucl. Energy* 140 (2021). <https://doi.org/10.1016/j.pnucene.2021.103904>.
- [20] Y. Ma, C. Tian, H. Yu, et al., Transient heat pipe failure accident analysis of a megawatt heat pipe cooled reactor. *Prog. Nucl. Energy* 140 (2021). <https://doi.org/10.1016/j.pnucene.2021.103904>.
- [21] G. Hu, R. Hu, J. Kelly, et al., Multi-physics simulations of heat pipe micro reactor. Tech. rep., Argonne National Lab.(ANL), Argonne, IL (United States), 2019, <https://doi.org/10.2172/1569948>.
- [22] C. Matthews, V. Laboure, M. DeHart, et al., Coupled multiphysics simulations of heat pipe microreactors using DireWolf. *Nucl. Technol.* 207, 7 (2021). <https://doi.org/10.1080/00295450.2021.1906474>.
- [23] Y. Yuan, J. Shan, B. Zhang, et al., Accident analysis of heat pipe cooled and AMTEC conversion space reactor system. *Ann. Nucl. Energy* 94 (2016). <https://doi.org/10.1016/j.anucene.2016.04.017>.
- [24] Z. Zhipeng, Y. Haoran, W. Haiping, et al., Neutronics and Thermal-hydraulics Analysis of Megawatt-class Level Heat Pipe Reactor. *Atomic Energy Science and Technology* 56, 9 (2022). <https://doi.org/10.7538/yzk.2021.youxian.0712>.
- [25] Y. Guo, Z. Li, K. Wang, et al., A transient multiphysics coupling method based on OpenFOAM for heat pipe cooled reactors. *Sci. China Technol. Sci.* 65, 1 (2022).

- 687 <https://doi.org/10.1007/s11431-021-1874-0>.
- 688 [26] C. Lee, Y. S. Jung, Development of the PROTEUS and ANSYS
689 coupled system for simulating heat pipe cooled micro reactors.
690 Tech. rep., Argonne National Lab.(ANL), Argonne, IL (United
691 States, 2020). <https://doi.org/10.2172/1601796>.
- 692 [27] D. I. Poston, M. A. Gibson, T. Godfroy, et al., KRUSTY
693 reactor design. Nucl. Technol. 206, sup1 (2020).
694 <https://doi.org/10.1080/00295450.2020.1725382>.
- 695 [28] J. H. Jang, A. Faghri, W. S. Chang, et al., Mathe-
696 matical modeling and analysis of heat pipe start-up from
697 the frozen state. ASME. J. Heat Transfer. 112, 3 (1990).
698 <https://doi.org/10.1115/1.2910427>.
- 699 [29] D. K. Edwards, V. E. Denny, A. F. Mills, Transfer processes.
700 an introduction to diffusion, convection and radiation, Series in
701 Thermal and Fluids Engineering (1978).
- 702 [30] J. K. Fink and L. Leibowitz, Thermodynamic and trans-
703 port properties of sodium liquid and vapor, Report (1995).
704 <https://doi.org/10.2172/94649>
- 705 [31] H. H. Coe, Summary of thermophysical properties of potas-
706 sium, Report (1965).
- 707 [32] J. E. Matsson, An introduction to ansys fluent 2023, (Sdc Pub-
708 lications, 2023).
- 709 [33] M. Ivanovski, V. P. Sorokin, I. V. Yagodkin, Physical principles
710 of heat pipes. (1982). <https://www.osti.gov/biblio/6148667>.
- 711 [34] M.-M. Chen, A. Faghri, An analysis of the vapor flow and
712 the heat conduction through the liquid-wick and pipe wall
713 in a heat pipe with single or multiple heat sources. Int. J.
714 Heat Mass Transfer 33, 9 (1990). [https://doi.org/10.1016/0017-9310\(90\)90226-K](https://doi.org/10.1016/0017-9310(90)90226-K).
- 715 [35] A. Faghri, M. Buchko, Y. Cao, A study of high-temperature
716 heat pipes with multiple heat sources and sinks: Part
717 I—Experimental methodology and frozen startup profiles. 113,
718 4 (1991). <https://doi.org/10.1115/1.2911193>.
- 719 [36] D. I. Poston, Space Nuclear Reactor Engineering, Tech. rep.,
720 Los Alamos National Laboratory (LANL). Los Alamos, NM
721 (United States, 2017). <https://doi.org/10.2172/1345963>.
- 722 [37] P. K. Romano, B. Forget, The OpenMC monte carlo
723 particle transport code. Ann. Nucl. Energy 51 (2013).
724 <https://doi.org/10.1016/j.anucene.2012.06.040>.
725